



Study on the Impact of Positioning Errors on the Process Performance of Robotic Bonnet Polishing

Xuepeng Huang¹ · Zhenzhong Wang¹ · Lucheng Li¹

Received: 30 April 2023 / Revised: 7 August 2023 / Accepted: 10 August 2023 / Published online: 2 September 2023
© The Author(s), under exclusive licence to Korean Society for Precision Engineering 2023

Abstract

High-precision optical components are widely used in major fields such as strong lasers and astronomy, but the production cycle of components is greatly constrained by the difficulty of machining optical components and the high price of special polishing machines, so it is important to develop a high-efficiency and low-cost fast polishing system for optical components. By combining bonnet polishing technology with industrial robotics, we have developed an industrial robotics bonnet polishing system for optical components, and the effect of robot positioning errors on pad trimming and on the polishing of the entire surface is also analyzed. To verify the processing capability of the robotic bonnet polishing device, polishing pad dressing experiments and optical component surface correction polishing experiments were carried out. After the pad was dressed, the runout value was reduced from 182 to 23 μm with a convergence ratio of 7.9. After polishing the optical component twice, the PV and RMS values on the surface of the component decreased significantly, from 38.05 λ and 9.98 λ to 8.65 λ and 1.38 λ ($\lambda=632.8$) respectively in the middle area of the component, with a convergence ratio of 4.4 and 7.2, proving that the robotic bonnet polishing system can be applied to the polishing process of optical components.

Keywords Bonnet polishing · Industrial robot · Positioning error · Pad dressing · Corrective polishing

1 Introduction

The dominant processing technology for large-diameter aspheric polishing is computer controlled optical surfacing (CCOS). It is a computer-controlled precision machine that uses contact or non-contact small tools to polish and finish the surface of the workpiece. There are many different types of CCOS technology. Such as bonnet polishing (BP) [1], magnetorheological finishing (MRF) [2], ion beam polishing (IBP) [3], small tool polishing (STP) [4], stressed-lap polishing (SLP) [5], and fluid jet polishing (FJP) [6]. The bonnet polishing technique was developed by ZEEKO and D.D. Walker of University College London [7]. The bonnet is a crown-shaped rubber with a certain inflation pressure as a polishing tool, which not only ensures a good fit between the polishing head and the surface of the polished workpiece but also controls the polishing efficiency and the surface quality of the polished workpiece by adjusting the pressure

inside the bonnet, which is suitable for polishing aspheric and free-form surfaces. Pan et al. [8] investigated the optimal motion for bonnet tool for the purpose of optimizing the polishing process of ultra-precision optics. Bonnet polishing technology has been successfully applied to polishing processes for astronomical telescope sub-apertures, artificial joints, optical precision molds, etc. [9]

In addition to the process and application of bonnet polishing technology research, there are also researchers on the bonnet polishing technology machine tools research and development of the corresponding bonnet polishing machine tools. Gao et al. [10] designed and developed bonnet polishing samples based on their research on bonnet polishing technology; Pan et al. [11] developed a bonnet polishing system and designed and manufactured the BP-2MK460 model bonnet polishing machine, which was successfully applied to the polishing of large diameter aspherical components. Bonnet polishing machine tools can meet the current needs of most aspheric and curved workpiece polishing processes, but as dedicated five-axis or more than five-axis linkage machine tools, the cost is relatively expensive. Therefore, more and more researchers are carrying out research related to robot-assisted polishing to reduce the cost of the equipment.

✉ Zhenzhong Wang
wangzhenzhong@xmu.edu.cn

¹ School of Aerospace Engineering, Xiamen University, Xiamen 361005, China

Six-axis industrial robots are used in a wide variety of engineering applications, such as handling, painting, and welding. Due to the high flexibility and relatively low price of industrial robots, researchers have developed a series of new polishing devices based on industrial robots in combination with commonly used polishing techniques. For example, robotic magnetorheological polishing [12, 13], robotic bonnet polishing [14–16], and robotic small tool polishing [17].

Although robotic bonnet polishing (RBP) technology has been applied to the rapid polishing process of optical components, the law of its positioning error on the finishing quality of the polishing pad on the bonnet surface and the polishing quality of the optical components is still unclear. To reveal the influence of robot positioning errors on processing, the longitudinal-latitude method was used to characterize the bonnet surface morphology and numerical simulation of the bonnet dressing process based on the kinematic model of polishing pad dressing. The paper also introduces random positioning error values for the polishing dwell points and conducts numerical simulations for whole surface polishing. Finally, the quality of the actual polishing pad dressing and the quality of the optical component of the robotic bonnet polishing system are experimentally investigated.

2 Numerical Simulation of the Dressing and Polishing Process for RBP

The multi-axis linkage structure of the industrial robot makes it have good flexibility and can be applied to complex spatial posture processing occasions, but due to the existence of mechanical assembly, reducer clearance, and other problems, the positioning accuracy of the industrial robot is much worse than the machine tool, five-axis bonnet CNC bonnet polishing machine tool positioning accuracy within 10 μm , the industrial robot positioning accuracy of 100 μm . the existence of errors will have an impact on the bonnet surface polishing pad. The existence of errors will have an impact on the actual polishing dwell point in the dressing and bonnet polishing process, so it is necessary to investigate the impact of positioning errors on the polishing pad dressing quality and polishing quality law.

2.1 Analysis of the Effect of Robot Positioning Errors on the Dressing of the Polishing Pad

The material removal mechanism of the bonnet polishing technique is that the pad brings the free abrasive particles from the polishing fluid into the contact area and applies pressure to the free particles, thus removing material from the surface of the workpiece. Therefore it is necessary to ensure that there are enough holes on the surface of the pad

to carry the abrasive particles in the polishing fluid to the contact area for material removal, but after a period of time the bonnet is used, the surface of the pad will wear out, resulting in fewer holes on the surface and less pressure on the contact area [18], as shown in Fig. 1a. After gluing the polishing pad to the surface of the bonnet, the runout value of the bonnet after gluing the pad is relatively large due to the non-uniformity of the glue coating and the initial undulating shape of the pad, which causes large fluctuations in the polishing force and affects the polishing quality. Therefore, the polishing pad needs to be dressed, and the corrected polishing pad is shown in Fig. 1b.

The common ways of dressing the polishing pads on the bonnet polishing machine tool are offline and in-situ, as shown in Fig. 2. The offline type is a pendulum axis rotating around the center of the bonnet sphere, and the linear axis is used to adjust the feed of the grinding wheel, thus realizing the dressing of the polishing pad [19]. However, the offline dressing method requires a high level of accuracy in the repeated clamping of the tool, and the repeated disassembly is time-consuming, so in-situ dressing is mostly used for bonnet dressing. In-situ dressing is done by keeping the position of the cup wheel unchanged and by linking the X-axis, A-axis, and B-axis feeds of the machine tool to achieve the dressing trajectory [20].

The in-situ dressing device of the robotic bonnet polishing system is shown in Fig. 3a. The dressing module consists mainly of a fixture, a grinding wheel, and a servo motor. During dressing, the dressing module is placed in a fixed position on the electromagnetic table, the bonnet axis is moved to the position of the center axis of the grinding wheel, then the bonnet is moved down to touch the surface of the grinding wheel, and finally the NC code is run to allow the bonnet to deflect around the Y axis to complete the dressing process. The kinematic model of the robot is shown in Fig. 3b, with the grinding wheel rotating around the Z-axis, the bonnet rotating around the Z-axis, and the deflecting motion around the Y-axis.

To analyze the effect of the robot's positioning error on the dressing accuracy of the polishing pad of the bonnet,

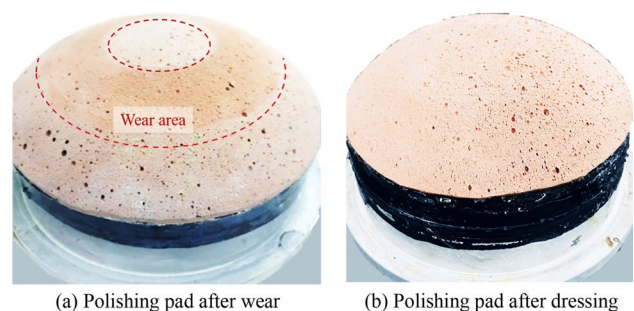


Fig. 1 Before and after polishing pad dressing

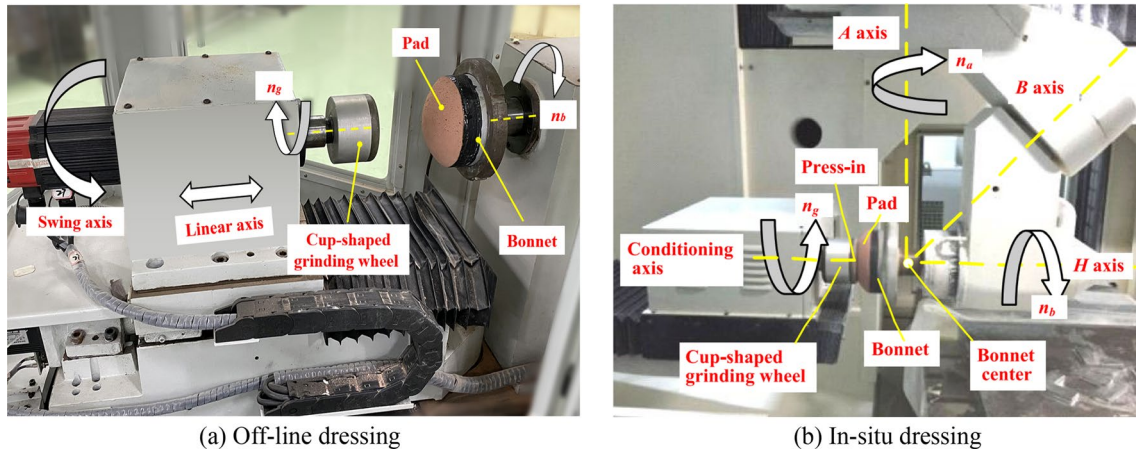


Fig. 2 Diagram of the pad dressing device

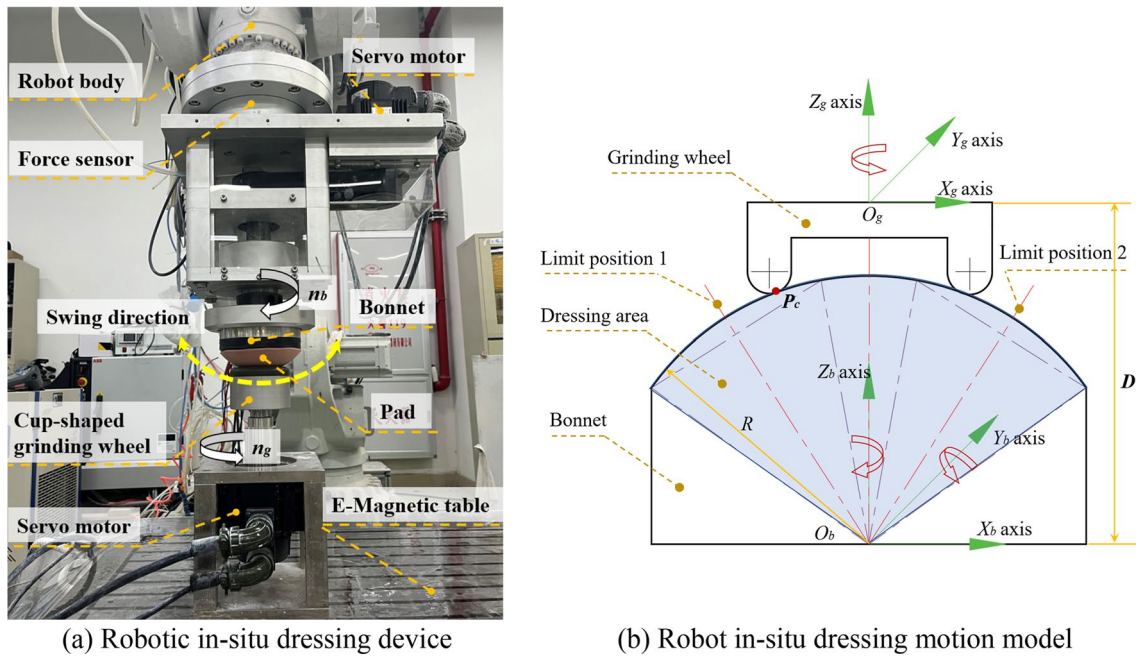


Fig. 3 Diagram of polishing pad dressing for RBP

the dressing process is numerically simulated according to the kinematic model of dressing. The kinematic modeling process is to assume that arbitrary point P on the grinding wheel is $P(x_g, y_g, z_g)$ in grinding wheel coordinates, then the real-time point position coordinates of point P on the surface of the bonnet during the dressing process is $P(x_b, y_b, z_b)$. The conversion process from $P(x_g, y_g, z_g)$ to $P(x_b, y_b, z_b)$ is shown in Eq. (1). The dressing process is where the coordinates of the polishing pad contact area are replaced with the coordinates of the grinding wheel after the wheel has passed over the surface of the pad.

$${}^bP = {}^bT_g P \tag{1}$$

where the transformation matrix bT_g is shown in Eq. (2).

$${}^bT_g = Rot(Y, \theta) Rot(Z, \beta) Trans(Z, D) Rot(Z, \alpha) \tag{2}$$

where the rotational transformation matrix is shown in Eq. (3), Eq. (4), and Eq. (5).

$$R_{gz} = \begin{pmatrix} \cos \alpha & -\sin \alpha & 0 \\ \sin \alpha & \cos \alpha & 0 \\ 0 & 0 & 1 \end{pmatrix} \quad (3)$$

where $\alpha = \omega_{gz} \cdot t$, $\omega_{gz} = 2 \cdot \pi \cdot n_{gz} / 60$, n_{gz} is the rotational speed of the grinding wheel.

$$R_{bz} = \begin{pmatrix} \cos(-\beta) & -\sin(-\beta) & 0 \\ \sin(-\beta) & \cos(-\beta) & 0 \\ 0 & 0 & 1 \end{pmatrix} \quad (4)$$

where $\beta = \omega_{bz} \cdot t$, $\omega_{bz} = 2 \cdot \pi \cdot n_{bz} / 60$, n_{bz} is the rotational speed of the bonnet.

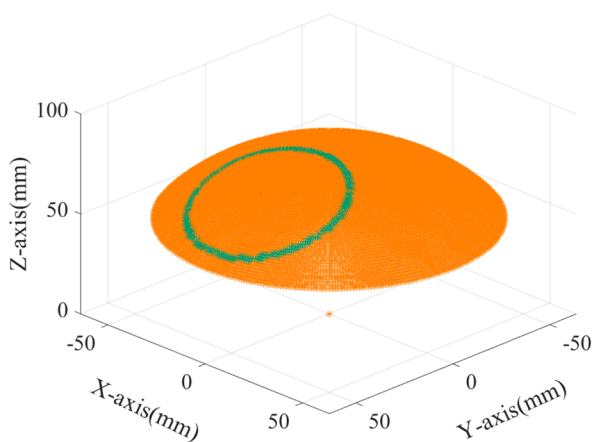
$$R_{by} = \begin{pmatrix} \cos(-\theta) & 0 & \sin(-\theta) \\ 0 & 1 & 0 \\ -\sin(-\theta) & 0 & \cos(-\theta) \end{pmatrix} \quad (5)$$

where $\theta = \omega_{by} \cdot t$, $\omega_{by} = 2 \cdot \pi \cdot n_{by} / 60$, n_{by} is the rotational speed of the bonnet swing.

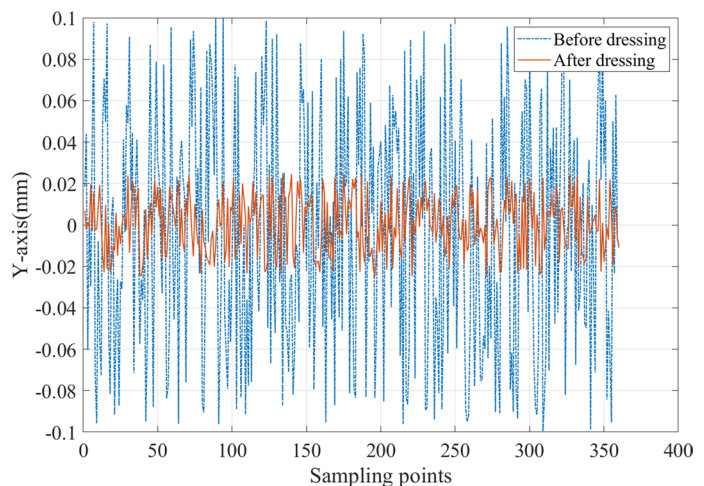
After obtaining the trimming kinematic model of the polishing pad on the bonnet surface, the bonnet surface topography is generated using the longitude latitude method, i.e. two angles and a radius value are used to characterize the bonnet, while a random value with the maximum value of the error value is added to the radius value. The simulation

Table 1 Process parameters for polishing pad dressing simulation

Bonnet radius (mm)	Grinding wheel diameter (mm)	Swing angle (°)	Number of dressing
80	60	60	2



(a) Numerical models



(b) Runout values before and after dressing

parameters are shown in Table 1, according to the actual initial surface error value to obtain a simulated numerical surface shape consistent with the actual polishing pad surface topography, as shown in Fig. 4a, where the orange dots represent the polishing pad and the green dots represent the grinding wheel. From the simulation results, it can be seen that the finishing accuracy of the polishing pad for robotic bonnet polishing is related to the positioning accuracy of the robot, taking the data of the ring band in the contact area between the bonnet and the workpiece, as shown in Fig. 4b, the runout in this area is slightly smaller than the robot's repeated positioning error, varies with random variations in positioning error. Therefore, the actual limit of the industrial robot's dressing accuracy can be subsequently verified through practical experiments.

2.2 Analysis of the Impact of Robot Positioning Errors on Polishing Quality

To analyze the impact of robot positioning errors on polishing quality, the simulation process assumes that the tool influence function (TIF) remains stable during the polishing process and that there is no error in the dwell time. The workpiece size for the simulation is 80 mm × 80 mm, the machining range is 60 mm × 60 mm, and a raster-type polishing path is used with a raster spacing of 1 mm and a dwell point step of 1 mm in the bonnet feed direction, where the calculation process uses a 0.1mm interval densification path and the diameter of the TIF is 20 mm, as shown in Fig. 5. Other process parameters for the simulation are shown in Table 2. Firstly, a simulation of the polishing process in the ideal condition, i.e. with zero positioning error, was carried out as shown in Fig. 6a. Then, a numerical simulation was

Fig. 4 Numerical simulation of polishing pad dressing

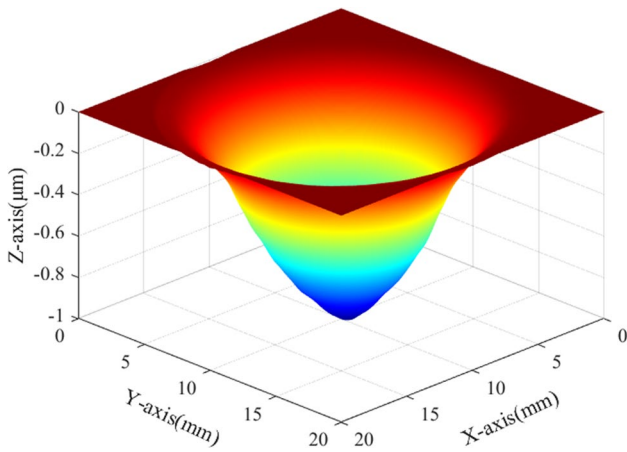


Fig. 5 Tool influence function

Table 2 Simulation parameters of bonnet polishing

Processing range (mm)	TIF size(mm)	Raster spacing(mm)	Time(s)
60*60	20	1	60

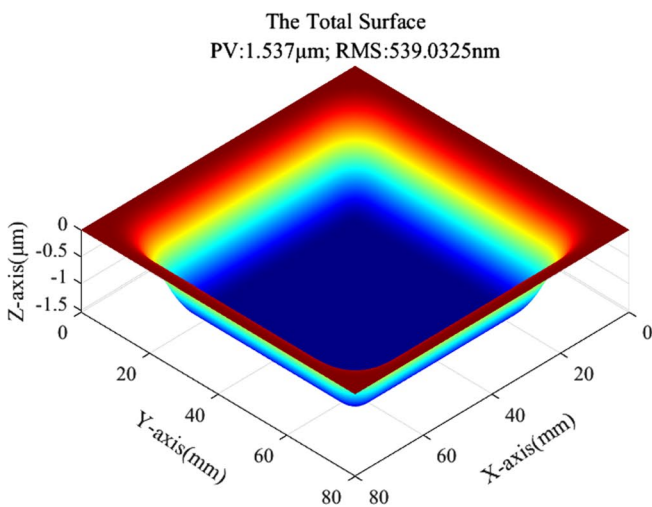
carried out with the robot positioning error, adding a random error of 0.1 mm to the stationary point, i.e. the stationary point could be positioned within a circle with the theoretical stationary point as the center and the random error as the radius, the simulation results are shown in Fig. 6b.

From the simulated surface, the maximum removal depth with and without positioning error is the same, so the positioning error of the robot does not have a large impact on the removal volume in the polishing process, which can indicate

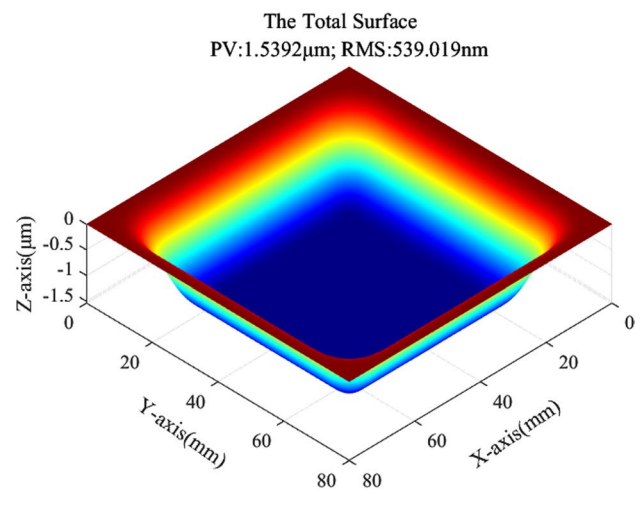
that the robotic bonnet polishing system can be applied to the fast polishing process of the polishing process. To better compare the effect of polishing quality with and without positioning errors, a polished area of 30 mm × 30 mm in the middle of the workpiece was selected for analysis, as shown in Fig. 7. The PV of the local area without positioning error is 0.99 nm and the RMS is 0.32 nm, while the PV of the intermediate local area after the introduction of robot positioning error is 5.8 nm and the RMS is 0.55 nm. This shows that the robot positioning error has a greater impact on the PV of the local surface shape and a smaller impact on the roughness.

As the robot positioning errors introduced by the simulation are random, the results of one simulation cannot objectively reflect the actual impact pattern. To better demonstrate the impact of random errors at the polishing point, five sets of simulations were carried out using the same process parameters, and the PV and RMS of each set were recorded as shown in Table 3.

Based on the above simulation strategy, we further investigate the influence of raster spacing and the TIF size on the polishing process under the trajectory motion error of the industrial robot. Firstly, numerical simulations of the raster paths were carried out using raster spacing of 0.5 mm, 1 mm, 1.5 mm, and 2 mm, and a TIF diameter of 20 mm, where the simulation was repeated five times for each raster path with positioning errors. At the end of the simulation, the PV and RMS data were selected for the middle local area and the results are shown in Table 4. The histogram of the simulation results with robot positioning errors is shown in Fig. 8, where the local PV and RMS increase as the raster spacing increases, and the ideal simulation results in Table 4 show that the local PV and RMS increase as the



(a) Simulation results without positioning error



(b) Simulation results with positioning error

Fig. 6 Simulation results of uniform polishing

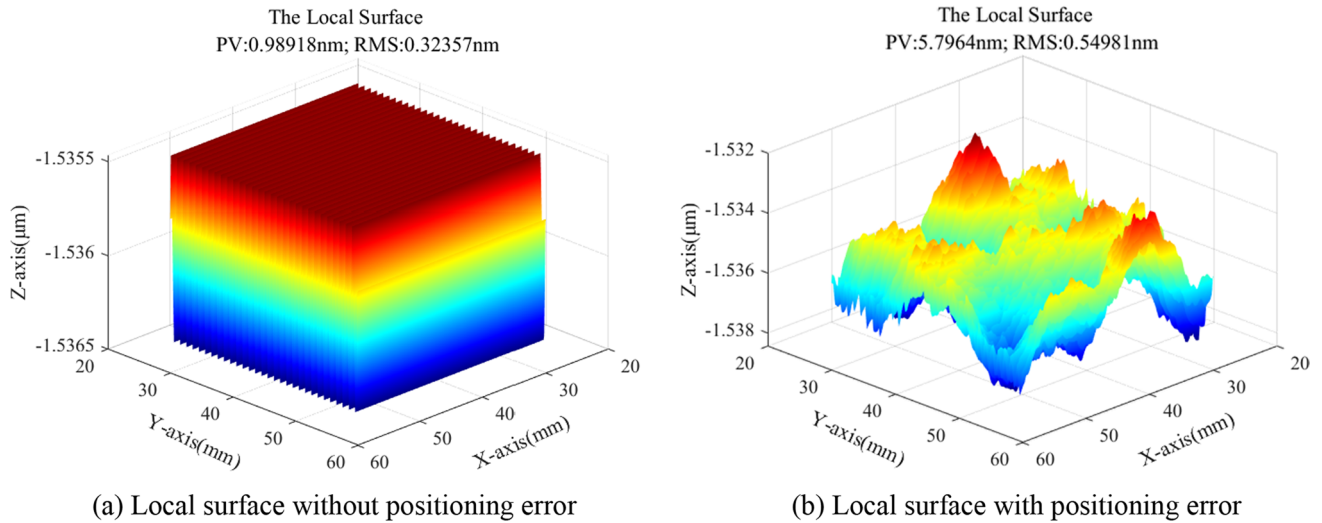


Fig. 7 Simulation results for local surfaces

Table 3 Results of repeated simulations

No	Total surface PV (μm)	Total surface RMS (nm)	Local surface PV (nm)	Local surface RMS (nm)
1	1.5395	538.998	6.664	0.943
2	1.5395	539.052	6.359	0.675
3	1.5409	539.026	8.128	1.141
4	1.5392	539.019	5.796	0.550
5	1.5398	539.009	8.495	0.997
Average	1.5378	539.019	7.088	0.861

raster spacing increases, so a raster spacing of 1mm or below can be used in the real polishing process.

In the numerical simulation of the whole surface polishing, in addition to the raster spacing, there is an important process parameter, which is the diameter of the TIF, so the effect of the diameter of the TIF on the local surface is studied with or without positioning error. Simulations were carried out using TIF diameters of 10 mm, 15 mm, 20 mm, and 25 mm and a raster spacing of 1mm, where a single set of simulations was carried out without positioning errors and

five sets of simulations were carried out with positioning errors.

The results of the five replicate simulations with positioning errors are shown in Table 5, and the trends are shown in Fig. 9, where it can be seen that as the size of the TIF increases, the local PV tends to decrease and the local RMS tends to increase, but the overall changes are small, so the raster spacing has a greater effect on the polishing quality than the diameter of the TIF. Another interesting phenomenon to note is that in the simulation without positioning error when the diameter of the TIF is 15 mm, the local PV and RMS are relatively small, but after adding the positioning error, there is no such characteristic, so in the actual polishing, this simulation result can be used for polishing with a 15 mm diameter TIF.

3 Experimental Results and Discussion

The above numerical simulation of the dressing process of the polishing pad and the results of the polishing numerical simulation show that the positioning error of the robot has a large impact on the quality of dressing and polishing, and

Table 4 Simulation results of different raster spacings

Raster spacing (mm)	PV without positioning error (nm)	RMS without positioning error (nm)	PV with positioning error (nm)	RMS with positioning error (nm)
0.5	0.120	0.044	3.769	0.522
1	0.989	0.324	7.088	0.861
1.5	1.138	0.415	10.573	1.271
2	4	1.285	16.522	2.110

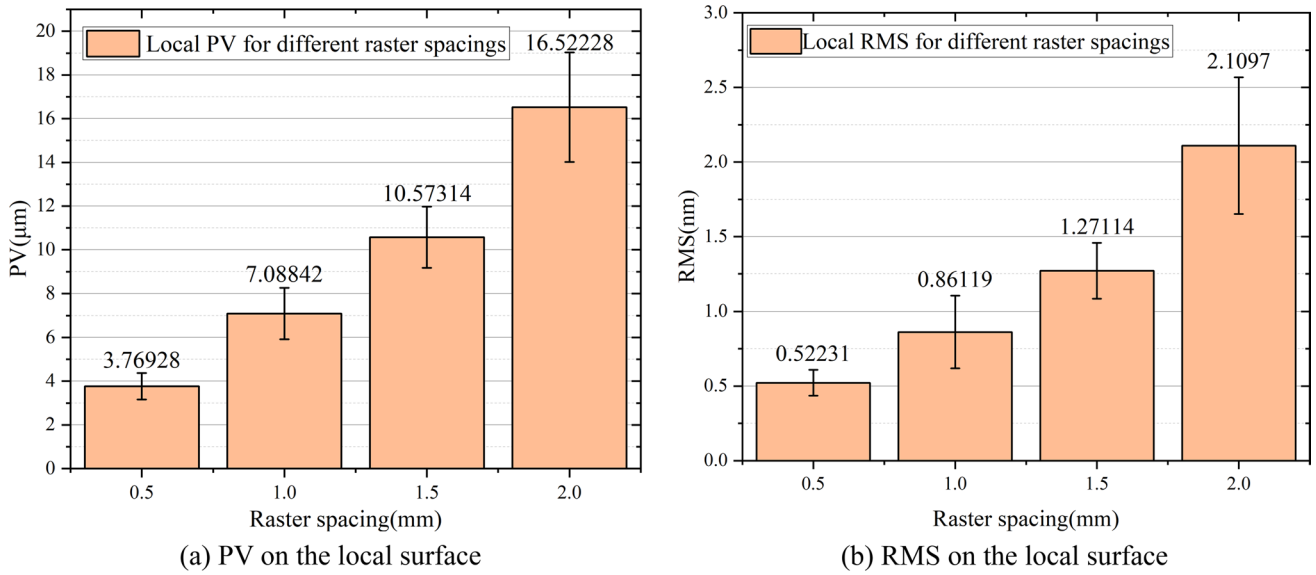


Fig. 8 Simulation results of different raster spacings

Table 5 Simulation results of different TIF

TIF diameter (mm)	PV without positioning error (nm)	RMS without positioning error (nm)	PV with positioning error (nm)	RMS with positioning error (nm)
10	0.908	0.317	7.870	0.678
15	0.464	0.148	7.240	0.773
20	0.989	0.324	7.088	0.862
25	0.799	0.270	6.996	1.006

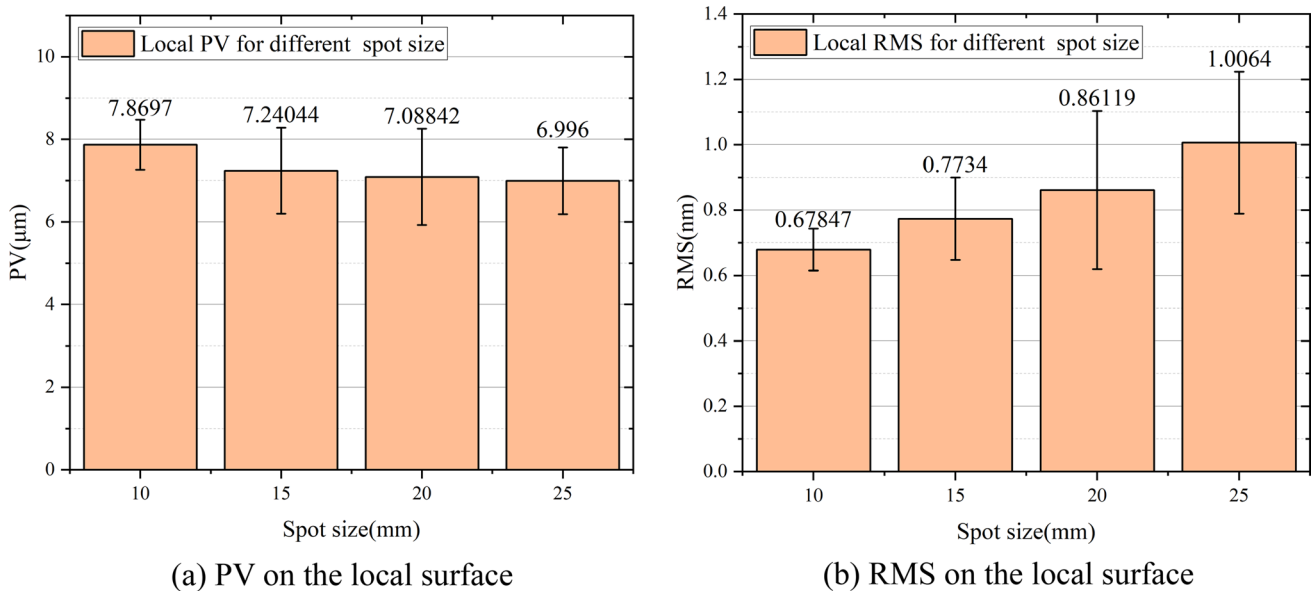
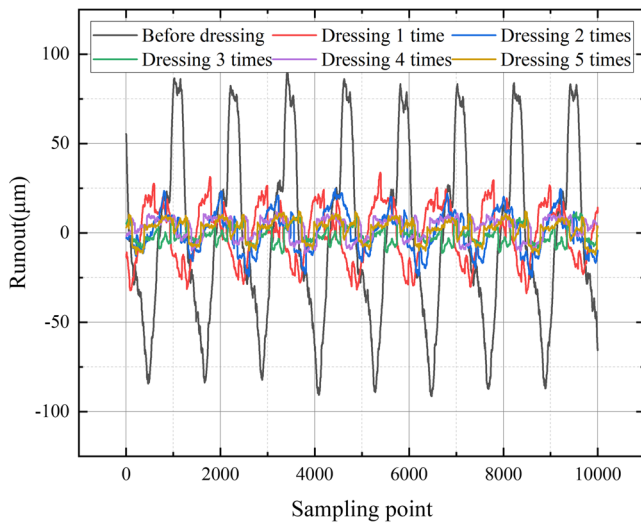
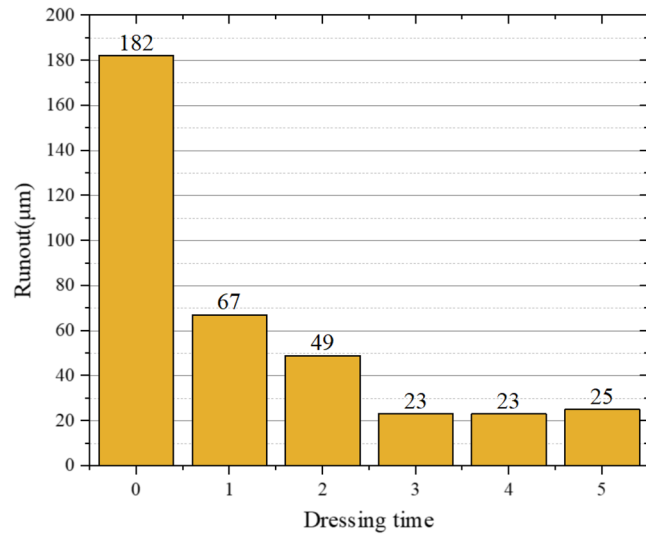


Fig. 9 Simulation results of different TIF



(a) Sampling points in the working area of the pad



(b) Runout values after dressing

Fig. 10 Data before and after polishing pad dressing

Table 6 Process parameters for dressing experiments

The rotational speed of the bonnet (rpm)	The rotational speed of the grinding wheel (rpm)	Swing angle (°)	Material of polishing pads
100	500	60	Polyurethane

the numerical simulation allows the scale of the impact of the positioning error to be known. Based on the numerical simulation, the polishing pad dressing experiment and the polishing experiment of optical components were carried out to investigate the processing accuracy of robotic bonnet polishing technology. The industrial robot selected for the experiments is ABB’s IRB6700 six-axis industrial robot with a positioning accuracy of 0.1 mm and a load capacity of 200 kg.

3.1 Results and Discussion of Pad Dressing Experiment

The process parameters for the polishing pad dressing experiments of the robotic bonnet polishing system are shown in Table 6. The bonnet speed and the grinding wheel speed are the key parameters, as shown in the results of the study by Pan [20, 21], the grinding wheel speed has to be much higher than the bonnet speed to have a better dressing effect. Heating up to set the shape. The polishing pad is then glued to the surface of the bonnet with soft glue. Based on the kinematic model for polishing pad dressing in Sect. 2.1, the

origin of the robot’s workpiece coordinate system is set at the center of the bonnet sphere. The machining points are then set uniformly within the swing range and the posture angles are converted to quaternions of the robot’s end posture through the robot’s transformation matrix. Later, an NC code is generated to start the dressing experiment. The instrument used to inspect the surface of the polishing pad was an LK-G10 laser displacement sensor from Keyence with an accuracy of 0.02 µm.

After three dressing experiments, as shown in the Fig. 10, The runout value of the polishing pad decreased from 182 to 23 µm. The further dressing did not change significantly after the fourth time but started to become larger after the fifth time. Therefore, the more appropriate number of dressings for robotic bonnet dressing is 3 times the process parameters shown in Table 6. And the dressing effect is good enough to suit the actual polishing requirements.

3.2 IRBP Correction Polishing Experimental Results and Discussion

Bonnet polishing is not only highly efficient for conformal polishing, but is also widely used for surface correction polishing of optical components, so we investigated the surface correction polishing capability of the robotic bonnet polishing system by conducting a correction polishing experiment on optical components. The NMF600S from Dutch United Instrument was used to measure the initial surface profile of the workpiece with an accuracy of 15 nm (RMS), which meets the measurement requirements. The initial RMS was

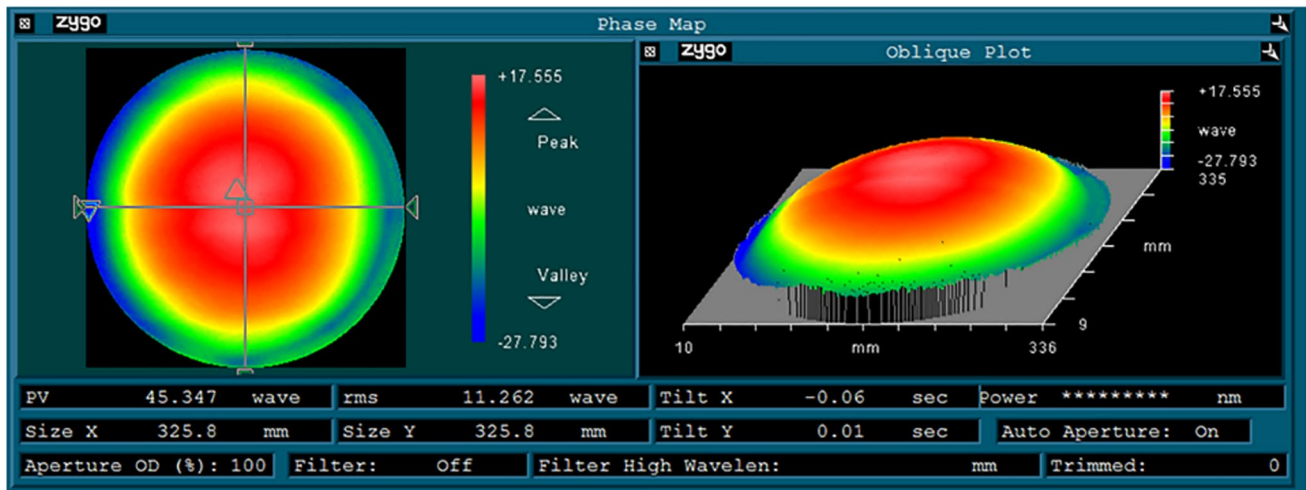


Fig. 11 Results of the initial surface measurement of the workpiece

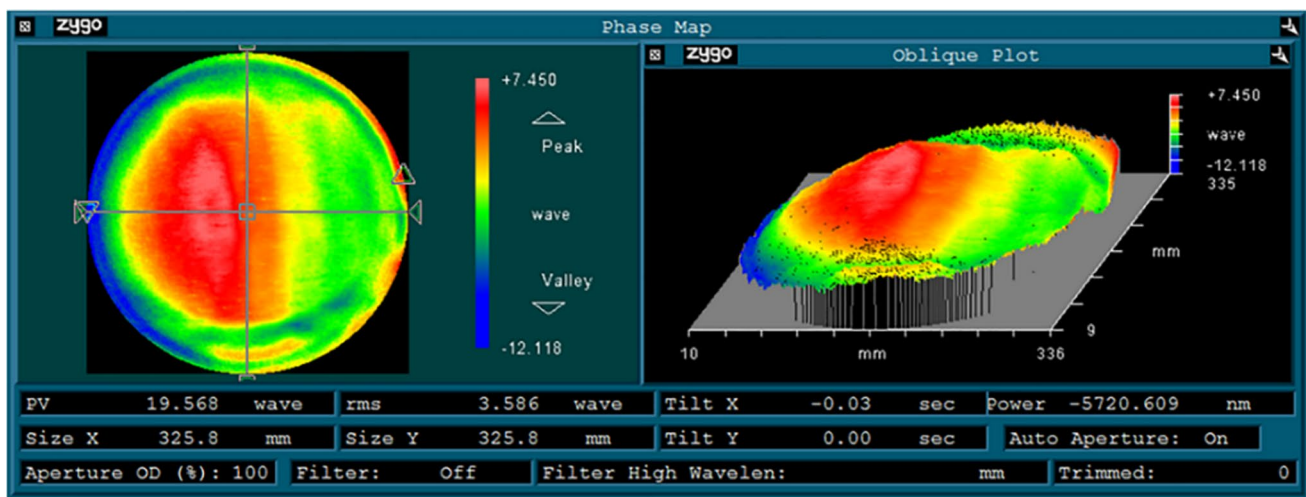


Fig. 12 Workpiece measurement after first polishing

11.26λ , the PV was 45.34λ ($\lambda = 632.8 \text{ nm}$) and the three-dimensional surface is shown in Fig. 11, with the workpiece having a high center and low sides.

For the processing path of round optical components usually use a spiral path or raster path, in this experiment we use raster path polishing, considering the bonnet polishing to the edge of the workpiece may cut the polishing pad, then in the edge of the workpiece reserved 5 mm, that is, the actual bonnet polishing area is $\varnothing 320 \text{ mm}$, to better surface quality, the raster spacing is set to 1mm. The TIFs used for the experiments were 20mm and 15mm in diameter.

The workpiece was polished using a TIF of $\varnothing 20$ for 118 min. After cleaning, the surface shape of the workpiece

was measured using the DUI NMF600S, and the results are shown in Fig. 12. The initial surface was high in the middle and low around, but after polishing the surface became high on one side and low on the other, which was analyzed to be caused by the placement error of the workpiece. The RMS of the workpiece surface decreased from 11.26λ to 3.586λ and the PV of 45.34λ to 19.568λ . The results show that bonnet polishing is highly effective in correcting the PV and RMS of the workpiece surface and effectively converging the surface of the workpiece.

The surface PV and RMS of the components after the first polishing decreased rapidly and the measured surface shape data was used as the initial surface shape error for the next

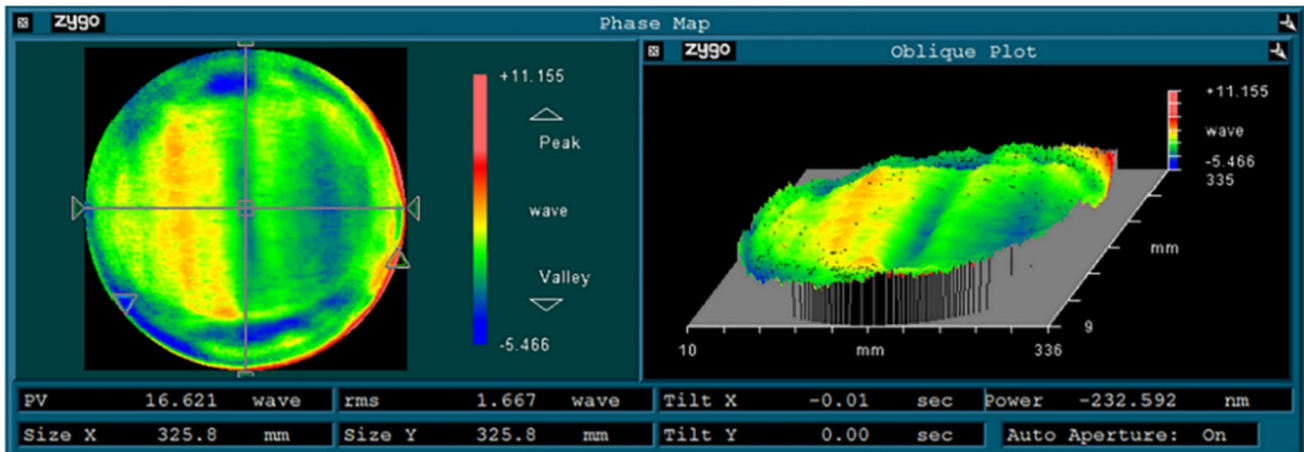
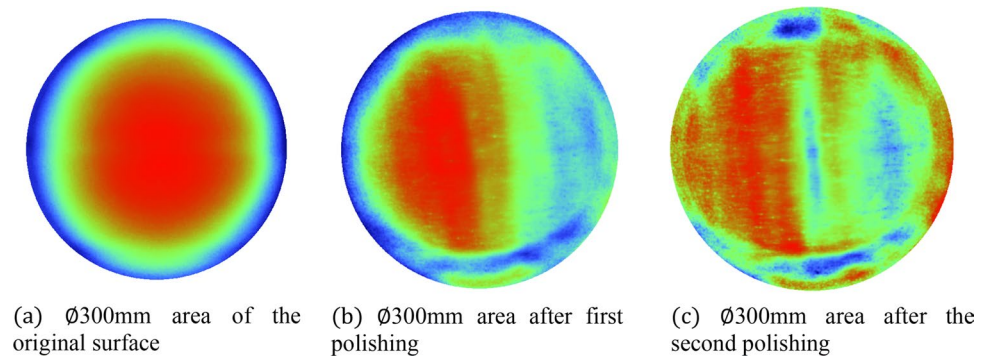


Fig. 13 Workpiece measurement after second polishing

Fig. 14 Comparison of measurement results in the middle area of the workpiece after polishing



process. The second polishing experiment was carried out using a Ø15 mm TIF with a processing time of 122 min. The polished components were cleaned and measured as shown in Fig. 13. As can be seen from the results, the RMS on the surface of the optical element drops from 3.59λ to 1.67λ , and the PV of 19.568λ drops to 16.62λ . Where the surface RMS continues to drop, but to a lesser magnitude, the edge effect of the element becomes apparent after the second polishing, resulting in a smaller decrease in PV.

To better demonstrate the polishing capability of the robotic bonnet polishing system, measurements of the workpiece Ø300 mm were intercepted, as shown in Fig. 14. The workpiece surface RMS decreased from 9.98λ to 1.38λ and the PV value of 38.05λ decreased to 8.65λ . The RMS convergence ratio was 7.2 and the PV convergence ratio was 4.4 during the polishing process, which proves that the robotic bonnet polishing system has good correction polishing ability and can quickly converge the surface. Therefore, the robotic bonnet polishing technology can be used for rapid and corrective polishing of optical components.

4 Conclusions

Robotic bonnet polishing technology is widely used in the rapid polishing process of various optical components because of its high removal efficiency. Robotic bonnet polishing affects the polished surface quality due to the low positioning accuracy of industrial robots. We reveal the relationship between robot positioning errors and the finishing quality of bonnet polishing pads and the polished surface quality of components. The main innovations of this paper are summarised as follows.

- (1) To analyze the influence of robot positioning accuracy on polishing pad dressing, we used the longitudinal-latitude method to characterize the polishing pad morphology on the bonnet surface, established a kinematic model of the bonnet dressing process, and carried out numerical simulations. The simulation results show that the accuracy of bonnet dressing is slightly less than the positioning accuracy of the robot. The final dress-

ing experiment was carried out and the polishing pad was dressed three times and the runout value decreased from 182 to 23 μm , which could meet the polishing requirements.

- (2) To analyze the effect of robot positioning accuracy on polishing, a random value less than the positioning error was added to the dwell point on the workpiece surface. The effect of different raster spacing and different diameter TIFs on polishing was compared by single-factor simulation. The results showed that the raster spacing has a large impact on the polishing quality, and the raster spacing should be chosen 1 mm and below. Finally, the polishing capability of RBP was verified by conducting polishing experiments on optical components. The results showed that the PV and RMS in the middle $\varnothing 300$ mm area of the workpiece decreased from 38.05 λ and 9.98 λ to 8.65 λ and 1.38 λ respectively, with a convergence ratio of 4.4 and 7.2, indicating that robotic bonnet polishing can be applied to the polishing process of optical components.

Acknowledgements This research was supported by the National Natural Science Foundation of China (No. 52075462)

Author contributions XH: Conceptualization, Methodology, Writing original draft, ZW: Supervision, Methodology, Funding acquisition. LL: Hardware development.

Data availability Data will be made available on request.

Declarations

Competing Interest The authors declare that they have no known competing financial interests or personal relationships that could have appeared to influence the work reported in this paper.

References

- Walker, D., Yu, G., Li, H., Messelink, W., Evans, R., & Beaucamp, A. (2012). Edges in CNC polishing: from mirror-segments towards semiconductors, paper 1: Edges on processing the global surface. *Optics Express*, 20(18), 19787–19798.
- Barman, A., & Das, M. (2018). Nano-finishing of bio-titanium alloy to generate different surface morphologies by changing magnetorheological polishing fluid compositions. *Precision Engineering-Journal of the International Societies for Precision Engineering and Nanotechnology*, 51, 145–152.
- Xiao, H., Dai, Y., Duan, J., Tian, Y., & Li, J. (2021). Material removal and surface evolution of single crystal silicon during ion beam polishing. *Applied Surface Science*, 544, 148954.
- Cheng, H., Dong, Z., Ye, X., & Tam, H. Y. (2014). Subsurface damages of fused silica developed during deterministic small tool polishing. *Optics Express*, 22(15), 18588–18603.
- Chen, M. Y., Feng, Y. T., Wan, Y. J., Li, Y., & Fan, B. (2010). Neural network based surface shape modeling of stressed lap optical polishing. *Applied Optics*, 49(8), 1350–1354.
- Beaucamp, A., Katsuura, T., & Takata, K. (2018). Process mechanism in ultrasonic cavitation assisted fluid jet polishing. *Cirp Annals-Manufacturing Technology*, 67(1), 361–364.
- Walker, D. D., Beaucamp, A. T., Brooks, D., Freeman, R., King, A., McCavana, G., Morton, R., Riley, D., & Simms, J. (2022). Novel CNC polishing process for control of form and texture on aspheric surfaces. In Proceedings of the SPIE, 4767, 99–105
- Pan, R., Zhang, Y., Ding, J., Huang, C., & Wang, Z. (2016). Optimization strategy on conformal polishing of precision optics using bonnet tool. *International Journal of Precision Engineering and Manufacturing*, 17(3), 271–280.
- Wu, Z., Shen, J., Peng, Y., & Wu, X. (2022). Review on ultrasonic bonnet polishing technology. *International Journal of Advanced Manufacturing Technology*, 121(5–6), 2901–2921.
- Xie, D. G., Gao, B., Yao, Y. X., & Yuan, Z. J. (2006). Movement modeling and simulation of precision mechanisms for bonnet tool polishing. *Journal of Mechanical Engineering*, 42(2), 101–104.
- Ri, P., Zhen-Zhong, W., Chun-Jin, W., Yin-Hui, X., Dong-Xu, Z., & Yin-Biao, G. (2014). Research on control optimization for bonnet polishing system. *International Journal of Precision Engineering and Manufacturing*, 15(3), 483–488.
- Xu, D., & Hu, T. T. (2023). Modelling and vibration control of magnetorheological-based polishing tool for robotic polishing process. *Mechanical Systems and Signal Processing*, 195, 110290.
- Zhang, L., Zhang, C., & Fan, W. (2022). Robotic magnetorheological finishing technology based on constant polishing force control. *Applied Sciences-Basel*, 12(8), 3737.
- Wang, C., Han, Y., Zhang, H., Liu, C., Jiang, L., & Qian, L. (2022). Suppression of mid-spatial-frequency waviness by a universal random tree-shaped path in robotic bonnet polishing. *Optics Express*, 30(16), 29216–29233.
- Zhong, B., Deng, W. -H., Chen, X. -H., Zheng, N. (2019) Precision manufacture of aspheric optics by robot-based bonnet polishing. In: *2nd Target recognition and artificial intelligence summit forum*, pp. 11427.
- Zhong, B., Xu, Q., Wang, J., Deng, W., & Chen, X. (2020). Evaluation and compensation of a kinematic error to enhance prepolishing accuracy for large aspheric surfaces by robotic bonnet technology. *Optics Express*, 28(17), 25085–25100.
- Wan, S., Zhang, X., Wang, W., Xu, M., & Jiang, X. (2019). Edge control in precision robotic polishing based on space-variant deconvolution. *Precision Engineering-Journal of the International Societies for Precision Engineering and Nanotechnology*, 55, 110–118.
- Shi, C., Peng, Y., Hou, L., Wang, Z., & Guo, Y. (2018). Improved analysis model for material removal mechanisms of bonnet polishing incorporating the pad wear effect. *Applied Optics*, 57(25), 7172–7186.
- Wang, Z., Wang, Q., Yang, X., Chen, S., Zhuang, X., & Peng, Y. (2017). Dressing scheme and process parameters analysis for bonnet tool in bonnet polishing. *Proceedings of the Institution of Mechanical Engineers Part C-Journal of Mechanical Engineering Science*, 231(19), 3569–3578.
- Pan, R., Tang, Y., Zhong, B., Chen, D., Wang, Z., Fan, J., & Zhang, C. (2019). Qualitative motion control optimization of the pad dressing process for bonnet tool. *IEEE-ASME Transactions on Mechatronics*, 24(3), 1141–1152.
- Pan, R., Hu, C., Xie, Y., Fan, J., Wang, Z., & Liu, Z. (2023). Study on optimization of process parameters in dressing of bonnet polishing tool. *Proceedings of the Institution of Mechanical Engineers Part B-Journal of Engineering Manufacture*. <https://doi.org/10.1177/09544054221150663>

Publisher's Note Springer Nature remains neutral with regard to jurisdictional claims in published maps and institutional affiliations.

Springer Nature or its licensor (e.g. a society or other partner) holds exclusive rights to this article under a publishing agreement with the author(s) or other rightsholder(s); author self-archiving of the accepted manuscript version of this article is solely governed by the terms of such publishing agreement and applicable law.



Xuepeng Huang received the B.S. degree from the College of Mechanical and Electrical Engineering, Fujian Agriculture and Forestry University, Fuzhou, China, in 2018, and the M.Eng. degree from the School of Aerospace Engineering, Xiamen University, Xiamen, China, in 2021. He is currently working toward the Ph.D. degree in the School of Aerospace Engineering, Xiamen University. His main research interests include robot-assisted machining and manufacture of advanced optical components.



Zhenzhong Wang received the B.S., M.S., and Ph.D. degrees from the Department of Mechanical and Electrical Engineering, Xiamen University, Xiamen, China, in 2003, 2006 and 2009, respectively. He is currently an associate professor of Xiamen University. He is mainly working on advanced optical ultra-precision equipment and processes, laser and additive processing and other related technologies.



Lucheng Li received his B.S. degree in Process Equipment and Control Engineering from Changzhou University, Changzhou, China, in 2021. He is currently working towards his M.S. degree in the School of Aerospace Engineering, Xiamen University, Xiamen, China. His main research interests include constant force control of robot in polishing.